Proceedings of ASME Turbo Expo 2020
Turbomachinery Technical Conference and Exposition
GT2020
June 22-26, 2020, London, England

GT2020-15541

PART LOAD STRATEGY DEFINITION AND PRELIMINAR ANNUAL SIMULATION FOR SMALL SIZE SCO_2 BASED PULVERIZED COAL POWER PLANT

Dario Alfani[1], Marco Astolfi[1], Marco Binotti[1], Paolo Silva[1]

[1] Department of Energy, Politecnico di Milano, Milano, Italy

ABSTRACT

In the near future, due to the growing share of variable renewable energy in the electricity mix and the lack of large-scale electricity storage, coal plants will have to shift their role from base-load operation to providing fluctuating back-up power. However, current coal power plants, based on steam Rankine cycle, are not optimized for flexible part-load operation, resulting in an intrinsic inadequacy for fast load variations. The founding idea of the H2020 sCO_2-Flex project is to improve the flexibility of pulverized coal power plants by adopting supercritical CO_2 Brayton power cycles. Despite the extensive literature about the design of sCO_2 plants there is still limited discussion about the strategies to be implemented to maximize system efficiency during part-load operation. This paper aims to provide deeper insight about the potential of sCO_2 power plants based on recompressed cycle with high temperature recuperator bypass configuration for small modular coal power plants (25 MWel). Analysis focuses on both design and part-load operation providing a preliminary sizing of each component and comparing different operating strategies. Results demonstrate that sCO_2 coal power plants can achieve competitive efficiency in both nominal and part-load operation thanks to the progressive increase of heat exchangers effectiveness. Moreover, they can be operated down to 20% electric load increasing power range of coal plants. Finally, the possibility to optimize the cycle minimum pressure ensures a safe operation of the compressor far from the surge line and to increase the performance at low load.

INTRODUCTION

Supercritical CO_2 cycles for power generation are gaining a large interest from industry, institutions and academia as demonstrated by the large amount of investments, funded projects and research papers. This interest is motivated by the potential of sCO_2 technology in replacing conventional steam cycles in a number of applications and likely playing a relevant role in the future energy scenario. The H2020 sCO2-Flex [1] project is studying the possible application of sCO_2 cycles in coal fired power plants in order to enhance their flexibility and ease the integration with non-dispatchable renewable energy sources such as wind and solar. Main advantages of sCO_2 power plants with respect to Ultra Super Critical (USC) steam cycle technology are: (i) potential higher efficiency, (ii) compactness of the turbomachinery, (iii) no need of water treatment, deaerator, vacuum pump, etc., (iv) high performance at part-load and (v) fast transients. The first two figures have been numerically evaluated in different independent studies [2]–[4] while the assessment of flexibility still lacks deep investigation. This study focuses on the steady state part-load performance and operational strategies for a sCO_2 cycle used as power cycle in a coal-fired power plant. Differently from closed Joule-Brayton cycles using for example He and N_2 that operate in the ideal gas region, in sCO_2 power cycles the main compressor is generally designed to operate very close to the fluid critical point in a region characterized by marked real gas effects (i.e. a region where the gas has a compressibility factor Z significantly lower than 1) [5]. For these systems, cycle depressurization at partial load may cause a significant variation of fluid properties along the compression with an efficiency penalization that may jeopardize also the overall plant performance. The optimization of the part-load operation of sCO_2 power plants is scarcely studied in literature and the main unknowns regard the design and the operation of turbomachinery. In this work, two different operating strategies are investigated for a recuperative

recompressed cycle configuration provided by High Temperature Recuperator (HTR) bypass selected within the sCO2-Flex project [6].

METHODOLOGY AND SYSTEM LAYOUT

More than 50 different sCO_2 cycle layouts have been proposed in literature [7] for different applications, showing large adaptability in terms of exploitation of different kind of heat sources and a consequent large range of applications spanning from solar, to waste heat recovery and fossil fuels [2][8][9]. The H2020 funded sCO2-Flex project aims to assess the potential of sCO_2 cycles coupled to coal-fired power plants providing a full understanding of the design of the components and the operational issues from both a steady state and a dynamic perspective. Within the project, twenty-one promising cycles configurations have been selected and optimized in order to identify the most suitable one for this specific application [10]. sCO_2 cycles are generally highly regenerative with a consequently limited variation of temperature across the primary heat exchanger: this characteristic leads to high cycle thermodynamic efficiencies thanks to the minimization of the irreversibilities in the internal heat transfer process, but it does not ease the coupling with a fossil fueled boiler as its efficiency can be penalized by a high stack temperature. The adoption of combustion air preheating with a Ljungström rotative heat exchanger mitigates only partially this problem, as the combustion air maximum temperature is generally limited to 350°C [11]. The plant overall efficiency (η_{plant}) is calculated as the product between cycle efficiency and boiler efficiency underlining the trade-off between these two figures of merit:

$$\eta_{plant} = \eta_{cycle}\eta_{boiler} = \frac{\dot{W}_{net}}{\dot{Q}_{in}}\frac{\dot{Q}_{in}}{\dot{Q}_{LHV}} = \frac{\dot{W}_{net}}{\dot{Q}_{LHV}} \quad (1)$$

Plant overall efficiency is hence greatly affected by the cycle configuration and it can be improved by adopting cycles configurations able to cool down flue gases to a lower temperature by limiting internal recuperative process. The selection, made by sCO2-Flex consortium, took in consideration i) the cycle performance, ii) the boiler integration and its thermal performance and iii) the system simplicity. Fig.1 depicts the recuperative recompressed cycle with High Temperature Recuperator (HTR) bypass that has been selected as the most appropriate layout for coal fired power plants.

This cycle, among the configurations selected within the sCO2-Flex project [6][10], is able to guarantee a higher boiler thermal efficiency thanks to a CO_2 stream that bypasses the HTR and that is heated up in the boiler, further cooling the flue gases. In addition, the presence of the secondary compressor allows to balance the heat capacities of the cold and hot CO_2 streams in the Low Temperature Recuperator (LTR), reducing the irreversibilities related to the heat exchange process. Similarly, the fluid split at HTR inlet allows reducing the temperature difference in this component thus increasing the cycle performance.

The coal-fired sCO_2 power plant nominal design and off-design performances have been evaluated with a numerical model specifically developed for the sCO2-Flex project, implemented in MATLAB [5] and adopting REFPROP 9.1 database [6] for the calculation of thermodynamic properties of CO_2. The code can be applied to any cycle configuration and after verifying mass and energy balances, it computes the cycle thermodynamic efficiency and carries out the preliminary sizing of the main components. The obtained results (e.g. heat exchanger areas, pressure drops, heat transfer coefficients, etc.), together with turbomachinery operative maps, are used as input data for the off-design simulation allowing to test different operating strategies and identify the most promising one from both flexibility and minimum attainable load perspective.

CYCLE THERMODYNAMIC DESIGN

Cycle configuration and assumptions

The analysis in the present study is carried out for a power plant having a plant net electric power output of 100 MW_{el}. Cycle maximum pressure and temperature are selected according to the current values adopted for Ultra Super Critical (USC) steam boilers and set to 250 bar and 620°C respectively [7]. Turbine and compressor efficiencies have been evaluated by Baker Hughes-General Electric, a partner of the sCO2-Flex consortium already involved in the STEP project as turbomachinery manufacturer [8].

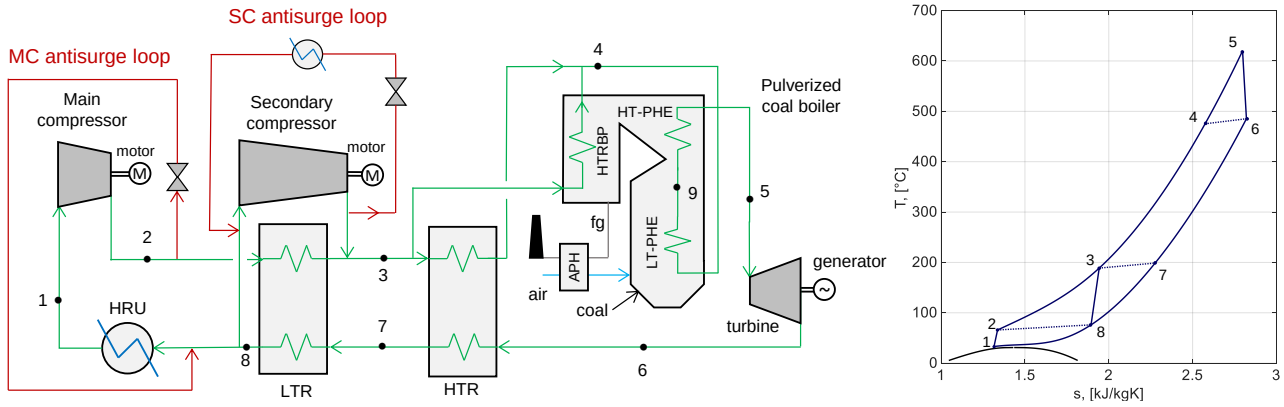

FIGURE 1: (left) schematic plant layout and (right) T-s diagram of the recompressed cycle with HTR bypass

The minimum cycle temperature is assumed equal to 33°C in order to exploit real gas effects of CO_2 and reduce main compressor work, while the minimum cycle pressure is optimized in order to maximise the cycle efficiency. A water-cooled heat rejection unit is considered in this work in order to limit the cycle efficiency penalization in the hot season. In fact, with dry air cooling, the main compressor inlet volumetric flow would dramatically increase with increasing ambient temperature, with a consequent difficulty in the efficient and stable operation of the compressor and the overall system [12][13]. In addition, an isothermal mixing process is assumed at both LTR and HTR outlet by acting on the split ratio at secondary compressor inlet and HTR-bypass respectively, thus guaranteeing no mixing irreversibilities. All the main assumptions for the cycle design are summarized in Table 1.

Cycle thermodynamic efficiency (η_{cycle}) is calculated considering the turbine and compressors works, the mechanical and electric efficiencies of turbine generator ($\eta_{me,t}$) and compressor motors ($\eta_{me,c}$) and the heat rejection auxiliaries consumption.

$$\eta_{cycle} = \frac{\dot{W}_{net}}{\dot{Q}_{in,cycle}} = \frac{\dot{W}_{CO2} - \dot{W}_{HRU,aux}}{\dot{Q}_{in,cycle}} \quad (2)$$

$$\dot{W}_{CO2} = \dot{W}_t - \dot{W}_{c1} - \dot{W}_{c2}$$

$$\dot{W}_{CO2} = \dot{m}_{CO2}\left[\Delta h_{5-6}\eta_{me,t} - SR\frac{\Delta h_{1-2}}{\eta_{me,c}} - (1-SR)\frac{\Delta h_{3-8}}{\eta_{me,c}}\right] \quad (3)$$

$$\dot{W}_{HRU,aux} = \dot{m}_w \frac{v\Delta p}{\eta_{pump}\eta_{me,p}} \quad (4)$$

$$\dot{Q}_{in,cycle} = \dot{m}_{CO2}[\Delta h_{4-5} + BR\ \Delta h_{3-4}] \quad (5)$$

In Eq. (3) the Split Ratio *SR* is defined as the fraction of CO_2 sent to the main compressor with respect to the overall CO_2 mass flow rate, while in Eq. (5) the Bypass ratio *BR* is defined as the fraction of CO_2 bypassing the HTR with respect to the overall CO_2 mass flow rate.

TABLE 1: Main assumptions for the cycle design

Cycle assumptions	
Plant design net electric power $W_{net,plant}$, MW_{el}	100
Maximum cycle temperature T_5,°C	620
Maximum cycle pressure p_2, bar	250
Minimum cycle temperature T_1,°C	33
Turbine isentropic efficiency, η_{turb}	89.8 %
Main compressor polytropic efficiency, η_{comp1}	77.7 %
Second. compressor polytropic efficiency η_{comp2}	76.7 %
Generator/motor mech.-electrical efficiency $\eta_{m,t}/\ \eta_{m,c}$	96.4 %
LTR pinch point ΔT_{LTR},°C	10
HTR pinch point ΔT_{HTR},°C	10
HRU CO_2 $(\Delta p/p_{in})$	0.5 %
Recuperators hot side $(\Delta p/p_{in})$	0.5 %
Cooling water pressure drop $\Delta p_{water,HRU}$, bar	1.5
Cooling water temperature increase $\Delta T_{water,HRU}$, °C	7
Cooling water pump efficiency η_{pump}	75%

Components design

Starting from the results of the thermodynamic optimization of the cycle and of the boiler, the preliminary design of the heat exchangers is performed, assuming the pressure drops provided in Table 1 as target.

As widely suggested in literature [9], Printed Circuit Heat Exchangers (PCHE) are adopted for both the LTR and HTR heat exchangers and their sizing is made in accordance with the work of Dostal [14] and with a set of hypotheses already used in previous works [10][13] and reported in Table 2. The recuperators are divided in 50 sections with a homogenous heat repartition and for each segment the overall heat transfer coefficient and pressure drops are calculated. The same number of straight channels is assumed for both hot and cold fluid and the design is found by matching the calculated value of hot fluid pressure drop with the assumed one. As result the cold fluid velocity is always lower than the hot one because of the higher pressure and pressure drops are around one order of magnitude lower suggesting that it would be beneficial to adopt multiple passes or non-straights channels in order to increase heat exchanger compactness. Eventually, the required heat transfer area, the metal mass and sCO_2 volumes are calculated.

TABLE 2: Main assumptions for PCHE design

Parameter	**Value**
Thickness of plate t_p, mm	1.5
Diameter of semi-circular channel d_c, mm	2
Thickness of wall between channels t_w, mm	0.4
Heat exchanger material	SS316

The heat rejection unit heat exchange area is computed considering a Shell and Tubes (S&T) heat exchanger with cooling water flowing in the shell side. A tube internal diameter equal to 20 mm has been adopted while the tube thickness has been computed through Eq. (6) considering a safety factor of 1.15. The main assumptions used for its design are reported in Table 3.

$$t = \frac{p d_{ext}}{2\sigma_{max} + p} + 0.005 d_{ext} \quad (6)$$

TABLE 3: Main assumptions for HRU design

Parameter	**Value**
Inlet water temperature, $T_{in,water}$, °C	20
Water temperature rise, ΔT_{water}, °C	7
External heat transfer coefficient, h_{ext}, W/m^2K	7500
Tube internal diameter, mm, d_i	20
Tube material	Cu

In order to provide the system with the highest flexibility at partial load, the turbine and the compressors shafts are independent. The expander is designed as a multistage axial turbine directly connected to the generator through a gearbox while each centrifugal compressor is connected to an independent variable speed motor. In addition, both compressors are equipped with VIGV ensuring a fast operation and enhanced operative range at part load.

BOILER THERMODYNAMIC DESIGN

The coal boiler is fuelled with reference BILINA HP1 coal having an ash-free chemical composition on a molar basis made by C: 37.85%, H: 34.81%, O: 9.16%, N: 0.40%, S: 0.25%, H_2O: 17.53% corresponding to a Lower Heating Value (LHV) equal to 16.9 MJ/kg. A closed coal drying system is assumed and coal water content enters the boiler with coal in vapour phase thus flue gas composition corresponds to coal as received. The excess of air in nominal condition is assumed equal to 20% with respect to the stoichiometric value in order to ensure complete combustion and to limit boiler stack losses. The adiabatic flame temperature is computed neglecting air staging and the stack temperature has been limited to minimum 130°C in order to avoid acid condenses caused by the formation of sulfuric acid (H_2SO_4) obtained from the reaction of sulfur trioxide (SO_3) and moisture in the flue gases. Other main assumptions are reported in Table 4.

Boiler efficiency (η_{boiler}) is calculated considering the heat loss of the flue gases at the stack as the only efficiency loss, thus neglecting heat losses from boiler walls to the environment and heat released with hot ashes:

$$\eta_{boiler} = \frac{\dot{Q}_{in,cycle}}{\dot{Q}_{LHV}} = 1 - \frac{\int_{T_{amb}}^{T_{stack}} \dot{m}_{fg} c_{p,fg}(T) dT}{\dot{m}_{fuel} LHV_{fuel}} \quad (7)$$

TABLE 4: Main assumptions for the boiler thermodynamic design

Boiler assumptions	
Ambient temperature, °C	25
Minimum allowable stack temperature T_{stack},°C	130
Minimum allowable boiler pinch point $\Delta T_{pp,boiler}$,°C	50
Minimum allowable Ljungström pinch point $\Delta T_{pp,Lj}$,°C	30
Boiler CO_2 side Δp_{boiler}, bar	2.5
Excess of air, ε	20%
Flue gas temperature at the radiative zone exit, $T_{out,rad}$, °C	1200
Maximum air temperature at LJ outlet, $T_{LJ,max}$, °C	350

The heat exchangers layout in the boiler is preliminary designed assuming co-current arrangement in order to limit the metal skin temperature and considering two different boiler zones as recommended by UJV partner in sCO2-Flex project [11]:

- A high temperature radiative zone where the main heat exchange mechanism is the radiation due to the presence of the flame and the high temperature of the flue gases. This zone includes the low temperature section of the Primary Heat Exchanger (LT-PHE) where the flue gases are cooled down to 1200°C. The LT-PHE is fed by pressurized sCO_2 after the mixing process at the outlet of HTR and it is designed as a membrane wall surrounding the combustion chamber. The value of the radiative heat flux on the membrane wall is computed through a series of Thermoflex [15][16] simulations of the radiant boiler component and its value is assumed equal to 116.9 kW/m^2.
- An intermediate-low temperature radiative-convective zone in which both radiation and convection are considered. In this zone the high temperature section of the Primary Heat Exchanger (HT-PHE) and the HTR bypass heat exchanger (HTRBP) are considered. The convective-radiative section (HT-PHE) is assumed as co-current flow tubular heat exchanger while the HTRBP heat exchanger is assumed as a counter-flow tubular heat exchanger, as the temperature of the flue gases has significantly decreased leading to a lower metal skin temperature. Both tubular heat exchangers in the boiler (HT-PHE and HTRBP) are discretized in 50 steps, each one exchanging the same amount of heat $\dot{Q}_j$. The internal heat transfer coefficient is computed with the Dittus-Boelter correlation [17], while the external heat transfer coefficient is computed as the sum of a convective and a radiative contribution, both estimated through correlation obtained from Thermoflex as function of the flue gases velocity and temperature [15][16].

The overall heat transfer coefficient referred to the internal area for the j-th step $U_{int,j}$ is then obtained as:

$$U_{int,j} = \left(\frac{1}{htc_{CO2,j}} + \frac{d_{int} \ln\left(\frac{d_{ext}}{d_{int}}\right)}{2k_t} + \frac{\frac{A_{int,j}}{A_{ext,j}}}{(htc_{FG,rad} + htc_{FG,conv})} \right)^{-1} \quad (8)$$

The internal heat transfer area of each heat exchanger in the radiative-convective section is finally computed as:

$$A_{int} = \sum_{j=1}^{50} \frac{\dot{Q}_j}{U_{int,j} \Delta T_{ml,j}} \quad (9)$$

Finally, the Ljungström air preheater, given its effectiveness from the thermodynamic design, is sized with Thermoflex deriving the average global heat transfer coefficient and heat transfer area. The main geometrical assumptions for the different boiler heat exchangers design are reported in Table 5.

TABLE 5: Main assumptions for boiler heat exchangers design

LT-PHE	
Tube internal diameter, mm	20
Ratio of tube pitch to external diameter	1.45
Tube and membrane material	INCONEL 617
HTR-BP and HT-PHE	
Tube internal diameter, mm	40
Ratio of tube pitch to external diameter	1.2
Ratio of transverse tube pitch to ext. diameter	10
Tube material	INCONEL 617

DESIGN RESULTS

The results of the thermodynamic design of the system are reported in Table 7. The obtained net cycle efficiency is 42.88%, while the boiler efficiency is 94.57%; combining these two contributions an overall efficiency of 40.55% is achieved. All the main thermodynamic properties of the optimal cycle streams are reported in Table 6.

TABLE 6: Thermodynamic streams of the sCO_2 cycle

Point	Temp. (°C)	Press. (bar)	Density (kg/m³)	Enthalpy (kJ/kg)	Entropy (kJ/kgK)
1	33.00	82.97	652.98	297.78	1.32
2	65.91	250.00	757.42	328.03	1.34
3	188.72	249.95	342.08	566.06	1.94
4	475.27	249.84	170.92	938.38	2.57
5	620.00	247.84	139.62	1120.04	2.80
6	485.27	84.22	58.38	966.86	2.82
7	198.72	83.80	101.40	636.81	2.28
8	76.01	83.38	175.29	482.02	1.89
9	567.17	248.57	149.50	1053.44	2.72

In order to maximize the boiler efficiency, stack temperature is pushed down to its lower bound value, while the air combustion temperature is increased at Ljungström exit with final values equal to the upper bound value (350°C). This involves that the pinch point temperature differences at the HT-PHE outlet section is higher than the minimum achievable technical value as also shown in Figure 2 that depicts the optimal boiler T-Q diagram. Table 8 reports the main results of the heat exchangers design showing how the two recuperators require large overall heat exchange areas due to the small ΔT_{LTR} and ΔT_{HTR} selected.

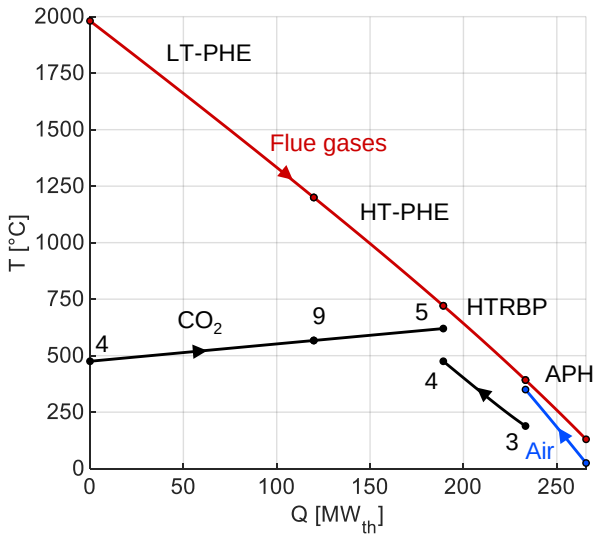

FIGURE 2: Boiler T-Q (temperature vs. thermal power exchanged) diagram.

TABLE 7: Main results of the boiler and cycle design

Boiler and cycle optimized results	
CO_2 mass flow at turbine inlet, kg/s	1041.54
CO_2 mass flow at HRU, kg/s	677.31
CO_2 mass flow at HTR bypass, kg/s	118.23
Split ratio SR	0.650
Bypass ratio BR	0.114
Minimum cycle pressure p_1, bar	82.97
Coal mass flow rate, kg/s	14.59
Air mass flow rate, kg/s	96.88
Flue gases mass flow rate, kg/s	110.12
Adiabatic flame temperature, °C	1980.96
Flue gases stack temperature, °C	130
Optimal boiler pinch point $\Delta T_{pp,boiler}$,°C	203.40
Ljungström pinch point $\Delta T_{pp,Lj}$,°C	42.12
Turbine electric power, MW_{el}	153.86
Main compressor electric power, MW_{el}	21.24
Secondary compressor electric power, MW_{el}	31.74
Heat rejection auxiliaries consumption, kW_{el}	878.05
Cycle efficiency	**42.88%**
Boiler efficiency	**94.57%**
Overall efficiency	**40.55%**

PART LOAD OPERATION

Components part load operation

The analysis of the system at part load is performed assuming a reduction of the fuel input and a corresponding correction of the combustion air mass flow rate according to the following correlation [11]:

$$\begin{cases} if\ \dot{Q}_{LHV} \geq 0.7\dot{Q}_{LHV,nom}\ ;\ \ \varepsilon = \varepsilon_{nom} \\ if\ \dot{Q}_{LHV} < 0.7\dot{Q}_{LHV,nom}\ ;\ \varepsilon = \varepsilon_{nom} + 0.7 - \dfrac{\dot{Q}_{LHV}}{\dot{Q}_{LHV,nom}} \end{cases} \quad (10)$$

Flue gases stack temperature is controlled through a variation of the Ljungström rotational speed thus changing its global heat transfer coefficient in order to maintain the stack temperature above the environmental limit.

For the considered preliminary analysis, a constant ambient temperature is assumed since the focus of the work is on the different operating strategies available for an active part-load control and consistent with the use of a water cooled HRU.

TABLE 8: Main results of the heat exchangers design

Parameter	HRU	LTR	HTR	LT-PHE	HT-PHE	HTRBP
Heat duty, MW	124.78	161.22	343.76	119.85	69.37	44.02
Hot side heat transfer coeff., W/m²K	8748.6	1577.1	1119.5	-	105.0	84.1
Cold side heat transfer coeff., W/m²K	7500	1509.0	1106.9	-	2920.7	1023.0
Global heat transfer coefficient, W/m²K	3911.6	747.3	545.8	116.1	97.1	73.9
Internal heat transfer surface, m²	1669.6	18801.4	43304.9	1682.9	1929.9	1978.9
CO_2 mass, kg (cold/hot)	3027	3028/757	3111/996	1344	2757	4734
HX metal mass, kg	19824	117240	270036	60713	119775	120339

As in design conditions, an isothermal mixing at the high pressure exit of the LTR and HTR is imposed by properly varying the split fraction to the secondary compressor and the one to the HTR bypass respectively. The maximum CO_2 temperature (T_5) is kept constant in order to simplify the analysis and avoid metal overheating in the furnace. The pressure drop in each heat exchanger section at part-load is corrected with respect to the design value through the following correlation:

$$\Delta p = \Delta p_{design} \left(\frac{\rho_{design}}{\rho}\right)\left(\frac{\dot{m}}{\dot{m}_{design}}\right)^2 \quad (11)$$

The heat transfer coefficients at part load operation on the CO_2 side for HTR, HTRB and LT-PHE and on the flue gas side for HTRB and LT-PHE are computed with a simplified approach as function of the ratio between the mass flow rate in off-design conditions and the mass flow rate in nominal operation:

$$htc_{CO2} = htc_{CO2,design}\left(\frac{\dot{m}_{CO2}}{\dot{m}_{CO2,design}}\right)^{0.8} \quad (12)$$

$$htc_{FG} = htc_{FG,design}\left(\frac{\dot{m}_{FG}}{\dot{m}_{FG,design}}\right)^{0.6} \quad (13)$$

The different exponents on the mass flow ratios for CO_2 and flue gases depend on the different correlations used for the calculation of the convective heat transfer coefficients [18].
In the LT-PHE, being the radiation the main heat exchange mechanism, the equivalent overall heat transfer coefficient U_{rad} computed in nominal conditions (see Table 8) is kept constant independently from the load as the variation of the adiabatic flame temperature is limited.
Finally, for the HRU and LTR, it has been preferred to compute the heat transfer coefficient with the proper correlations due to the proximity to the CO_2 critical point.
Cooling water flow rate and is calculated in order to maintain the compressor inlet temperature at design value. Cooling water pressure drop are varied according to Eq. (11), checking also that the temperature rise does not overcome environmental protection limits. HRU pump consumption is calculated accordingly.
Compressor off-design optimal operation is evaluated with a performance map derived by the manufacturer performance data as function of shaft speed and VIGV closing degree. The nondimensional map for the main compressor is reported in Figure 3 as function of the inlet volumetric flow rate ratio $\dot{V}_{in,comp}/\dot{V}_{in,comp,nom}$ and the enthalpy rise ratio in the component $\Delta h_{comp}/\Delta h_{comp,nom}$. For operative points different than the nominal one it is convenient to operate the compressor close to the surge line by varying the shaft rotational speed and adopting VIGV control only at very low or very high volumetric flow rates.

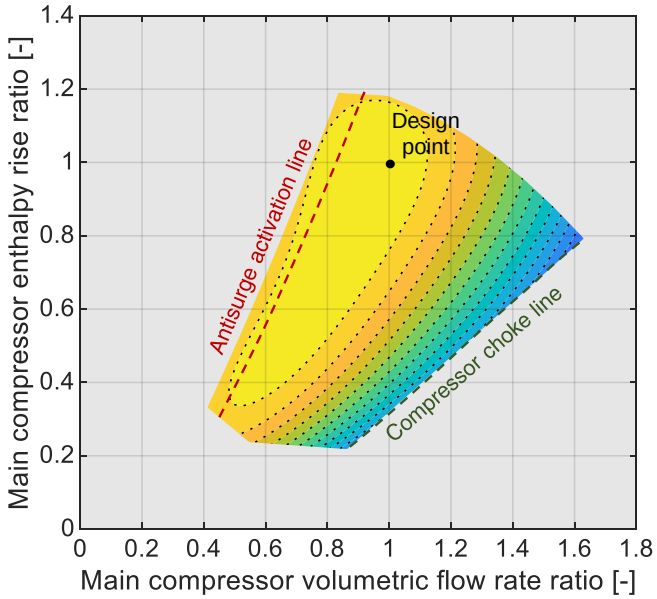

FIGURE 3: Dimensionless operational map of the main compressor.

In order to preserve compressor operability and lifetime it is important to avoid surge: in the model if the volume flow rate required to the system is lower than 1.1 times the corresponding surge limit value, the anti-surge bypass valve is opened ensuring stable compressor operation but increasing its consumption and thus penalizing system efficiency. The two compressor anti-surge loops are reported in Figure 1, left.
Turbine performances are evaluated with two part-load curves provided by the same manufacturer of the compressors: the first curve correlates the turbine pressure ratio with its flow coefficient ϕ reported in Eq. (14), the second links the isentropic efficiency of the component to its pressure ratio. Turbine efficiency remains very close to the nominal value unless the pressure ratio strongly decreases and the turbine moves from chocked conditions to the non-chocked conditions described by Stodola law.

$$\phi = \frac{\dot{m}_5\sqrt{T_5}}{p_5 A_{in,turb}} \quad (14)$$

Part load operation strategies
Different options are available for the part-load strategy of the cycle, depending on the turbomachinery features: compressors and turbine may be equipped with Variable Inlet Guide Vanes (VIGV) and may be able to vary their rotational speed. Moreover, a further option available in closed gas cycles is related to the possibility of varying the working fluid inventory thus changing the operating pressure of the system.
For the part-load operation two operational strategies have been investigated, as they were already highlighted as the most promising ones in precedent works [10][17].

The following cases are identified:

- CASE 1: Turbine in sliding pressure and fixed minimum cycle pressure equal to the design value, namely the thermodynamic condition at the inlet of the main compressor does not change in part-load;
- CASE 2: Turbine in sliding pressure and variable minimum cycle pressure in order to optimize plant efficiency.

The power plant operation has been simulated in steady state conditions for an electrical load ranging from 100% to 20%, as this is the expected functioning range for future small size coal fired sCO_2 power plants.
The study of transients, as well as start-up and shutdown, will be considered in future studies.

PART LOAD OPERATION RESULTS

Figure 4 shows the trend of the optimal minimum pressure of CASE 2 together with the values of pressure ratios for CASE 1 and CASE 2. In CASE 1 the cycle pressure ratio decreases because of the sliding pressure operation of the turbine and consequent reduction of maximum pressure. In CASE 2 this effect is partially compensated by the reduction of the minimum cycle pressure that decreases from 83 bar at nominal load to 77 bar at minimum load.

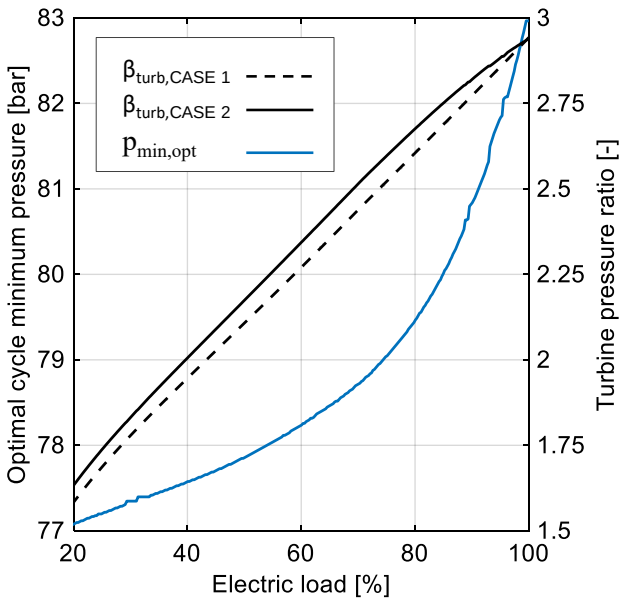

FIGURE 4: Trends of the optimal cycle minimum pressure and turbine pressure ratio for CASE 1 and CASE 2

Figure 5 depicts the trend of cycle efficiency, boiler efficiency and the plant efficiency for the two investigated part-load operational strategies. For both the cases, cycle efficiency tends to remain almost constant for a wide range of electrical load as the negative effect related to the reduced cycle pressure ratio with consequent reduction of the net cycle specific power output is compensated by the increased effectiveness of the heat exchangers. In fact, at part-load the heat exchangers are oversized with respect to their heat duty and consequently perform more effectively working with smaller temperature differences. For thermal power inputs below 70% of the nominal value, it is possible to notice a drastic change in boiler efficiency: the combustion air excess at boiler inlet is increased as specified in Eq. (10) and as a consequence the stack losses of the boiler increase remarkably. On the other hand, at around 60% of load the cycle thermodynamic efficiency starts to drop due to the excessive decrease of the cycle pressure ratio which has the double effect of departing more and more from its optimal value and also causing a decrease in the turbine isentropic efficiency.

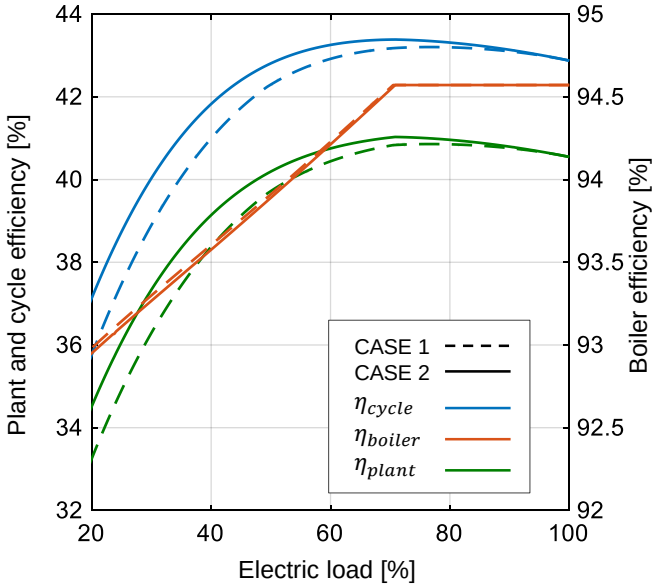

FIGURE 5: Trends of the cycle efficiency, boiler efficiency and plant efficiency as function of the electrical load

Figure 6 and Figure 7 report the main and the secondary compressor operating points as function of the electrical load for CASE 1 and CASE 2 on a dimensionless $\Delta h - \dot{V}$ chart. Line on the top left represents the surge limit, while the activation of the antisurge loop occurs with a safety margin equal to 10% of this value. It is possible to notice from Figure 6 that, adopting CASE 1 part-load operating strategy, the compressor operating tends to shift to the compressor surge line. At 50% of the electrical load the antisurge loop is already activated, with a decrease in the overall efficiency of the cycle due to the increased flow that the turbomachinery has to process.
For CASE 2, the minimum pressure changes with the electrical load allowing increase of the compressibility factor at the compressor inlet and keeping the operative point in the high efficiency region of the map at all times. The operating points of the secondary compressor reported in Figure 7 do not show criticalities, not imposing additional constraints to the power plant operation.

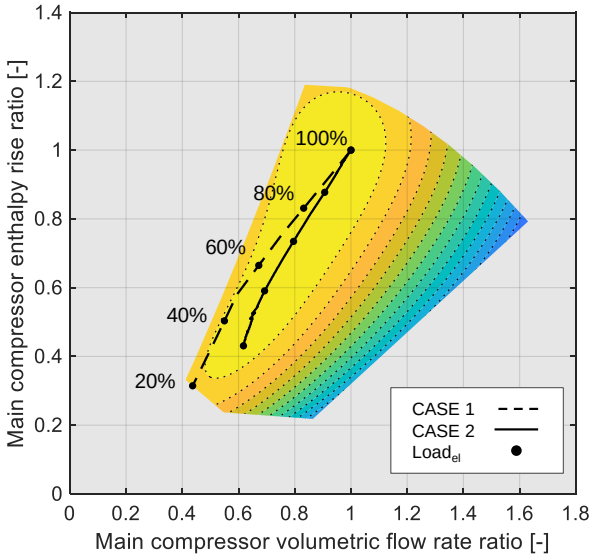

FIGURE 6: Main compressor operating points for the fixed minimum cycle pressure equal to the nominal value (CASE 1) and for optimal minimum pressure case (CASE 2) as function of the electrical load.

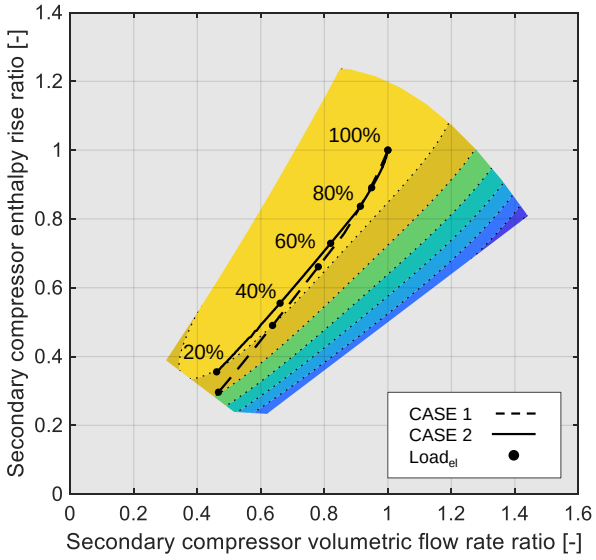

FIGURE 7: Secondary compressor operating points for the fixed minimum cycle pressure equal to the nominal value (CASE 1) and for optimal minimum pressure case (CASE 2) as function of the electrical load.

ANNUAL RESULTS

From historical power production data, it is evident that, except from some niche market where coal is abundant and cheap or where renewable energies contribution is low, USC coal power plants are experiencing a continuous reduction of their annual capacity factor. This is true for the United States [20][21], for Europe [22] and for Australia [23] where the participation to the electricity market of large coal power plants is limited by the progressive increase in renewable energy. In particular, the rapid increase of solar photovoltaic and wind energy arises issues related to frequency stabilization on the grid because of the random behavior of non-predictable renewable energy sources (NP-RES). In order to face the large fluctuation of power output of NP-RES it is crucial to rapidly act with the available power plants in operation and to promptly react to power shortcomings or overproductions. Large coal power plants (600-800 MW_{el}) show slow transients (4% nominal load/min), they cannot be started up and shut down rapidly- 5h for cold start (>72 hours off) and 2.5h from hot start (<8 hours off) and they are not adequate to play a balancing role in the future energy market as already demonstrated by recent years historic trends. On the contrary, natural gas fired combined cycles and gas turbines can provide a flexible and efficient solution to this problem but require an expensive fuel and have a less competitive LCOE. The proposed solution for future scenarios characterized by a larger NP-RES share is based on small coal fired sCO_2 power systems plants with a size between 25 and 100 MW_{el}, which can have an active role in the ancillary service market thanks to their flexibility and minimum achievable load, competing economically against gas turbines in compensating the fluctuation of NP-RES. In order to investigate the potential of this solution, a simplified national market model is implemented based on the hourly power demand and generation profiles for the Italian market and considering as renewable energies photovoltaic, wind, hydro and geothermal energy in the 2017 reference year [24]. The missing generating power is provided by a combination of coal and gas turbine power plants. The synthetic case obtained is not representative of a specific market but can provide first order estimation of the load frequency distribution under different scenarios.

Figure 8 depicts the load distribution for a USC steam coal power plant in current energy market scenario (left) where the share of NP-RES is not sufficient to strongly limit the operation of coal fired systems. On the contrary, the future scenario (middle) considers a progressive decommissioning of coal fired plants and an increase of the renewables share in the electricity mix, from 32% to 51%, obtained by multiplying by 3 the reference case solar photovoltaic energy production and by 2 the wind energy production.

These changes limit the operation of large coal power plants during high NP-RES availability hours since they cannot be switched off and they must run several hours at minimum load.

Switching from USC to sCO_2 would allow reducing the size of the plant, decreasing the minimum number of hours of continuous operation and extending the minimum load down to 20%: as shown in Figure 8-right the frequency of nearly nominal load hours increases and the whole operative range is exploited.

The obtained average annual efficiency (40.51%) is nearly equal to the nominal point thanks to the limited performance penalization in part load while energy curtailment reduces from 4.4% to 2.2% thanks to the higher flexibility of sCO_2 power plants [25].

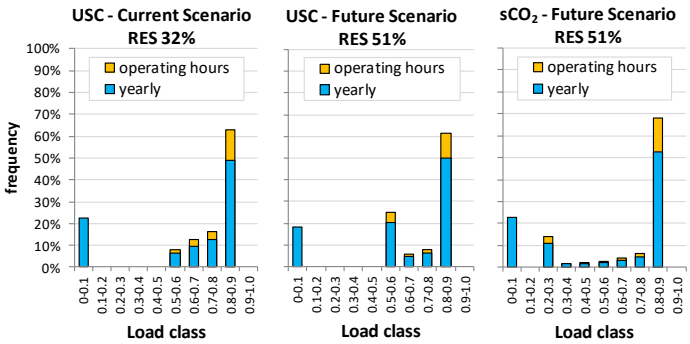

FIGURE 8: Load frequency distribution for coal USC power plants in the current (left) and in a future (middle) scenario and for small coal sCO_2 (right) power plants in a future scenario with high RES penetration.

CONCLUSIONS

In the present work, the study of a recuperative recompressed sCO_2 cycle with HTR by-pass as power cycle for a coal-fired power plant was performed. The achieved cycle efficiency is 42.88% and the overall plant efficiency 40.55%. Once a preliminary design of all the main heat exchangers was performed, two part-load operating strategies were compared in order to identify their impact on the plant efficiency and on the operating points of the main and secondary compressor. If the turbine works in sliding pressure the plant efficiency slightly increases down to 70% of the load and then decreases. The optimization of the minimum cycle pressure has limited impact on the plant efficiency (0.7 percentage points at 30% of the fuel input) but can facilitate the operation of the main compressor. Preliminary annual simulations confirmed that reducing the size of the plant allows to increase the number of operating hours at maximum load and to exploit the larger flexibility and minimum load capability of sCO_2 power plants. Future development of this work will include the study of the impact of the turbomachinery efficiency variation with the operating conditions and will investigate further operational degrees of freedom such as variation of the split ratio or of the HTR bypass ratio.

NOMENCLATURE

List of symbols

A	heat transfer surface area
c_p	specific heat
d	tube diameter
ε	Excess of air
η	efficiency
h	specific enthalpy or heat transfer coefficient
k_t	metal conductivity
$\dot{m}$	mass flow rate
p	pressure
$\dot{Q}$	heat
q	heat flux
ρ	density
σ	maximum allowable metal stress
s	specific entropy
T	temperature
U	global heat transfer coefficient
$\dot{W}$	power

List of subscripts

c	compressor
fg	flue gas
me	mechanical electric
pp	pinch point (temperature difference)
rad	radiative
t	turbine

List of Acronyms

APH	Air Preheater
BR	Bypass Ratio
CSP	Concentrated Solar Power
HT-PHE	High Temperature Primary Heat Exchanger
HTR	High Temperature Recuperator
HTRBP	High Temperature Recuperator Bypass
HRU	Heat Rejection Unit
LHV	Lower Heating Value
LT-PHE	Low Temperature Primary Heat Exchanger
LTR	Low Temperature Recuperator
PCHE	Printed Circuit Heat Exchanger
SR	Split Ratio
USC	Ultra Super Critical
VIGV	Variable Inlet Guide Vanes

ACKNOWLEDGMENTS

The sCO_2-Flex project has received funding from the European Union's Horizon 2020 research and innovation programme under grant agreement N° 764690

REFERENCES

[1] "SCO2-flex. [Online]. Available: http://www.sco2-flex.eu/." .

[2] M. Astolfi, D. Alfani, S. Lasala, and E. Macchi, "Comparison between ORC and CO2 power systems for the exploitation of low-medium temperature heat sources," *Energy*, vol. 161, pp. 1250–1261, Oct. 2018.

[3] T. Neises and C. Turchi, "A Comparison of Supercritical Carbon Dioxide Power Cycle Configurations with an Emphasis on CSP Applications," *Energy Procedia*, vol. 49, pp. 1187–1196, Jan. 2014.

[4] M. Mecheri, "SCO2 closed Brayton cycle for coal-fired power plant," *2nd Eur. Supercrit. CO2 Conf.*, pp. 0–8, 2018.

[5] G. Angelino, "Real gas effects in carbon dioxide cycles," 1969.

[6] M. Mecheri and S. Bedogni, "D1.3 – Report on the selected cycle architecture," no. August 2018, 2018.

[7] F. Crespi, G. Gavagnin, D. Sánchez, and G. S. Martínez,

"Supercritical carbon dioxide cycles for power generation: A review," *Applied Energy*, vol. 195. pp. 152–183, 2017.

[8] Y. Ahn *et al.*, "Review of supercritical CO2 power cycle technology and current status of research and development," *Nucl. Eng. Technol.*, vol. 47, no. 6, pp. 647–661, Oct. 2015.

[9] K. Brun, P. Friedman, and R. Dennis, *Fundamentals and Applications of Supercritical Carbon Dioxide (SCO2) Based Power Cycles*. 2017.

[10] M. Mecheri, "D1.1 – sCO2 Brayton cycle architecture and components' specifications," no. April 2018, 2018.

[11] J. Opatril, P. Hajek, and Z. Vlcek, "D2.3 – Boiler Modelling Report," no. June 2019, 2019.

[12] D. Alfani *et al.*, "Sizing Criteria and Performance Evaluation of Direct Air Cooled Heat Rejection Units for Supercritical CO2 Power Plants," in *5th International Seminar on ORC Power Systems, September 9 - 11, 2019, Athens, Greece*, 2019, pp. 1–9.

[13] D. Alfani, M. Astolfi, M. Binotti, P. Silva, and E. Macchi, "Off-design Performance of CSP Plant Based on Supercritical CO2 Cycles," in *SOLARPACES 2019: International Conference on Concentrating Solar Power and Chemical Energy Systems*, no. i.

[14] V. Dostal, M. J. Driscoll, and P. Hejzlar, "A Supercritical Carbon Dioxide Cycle for Next Generation Nuclear Reactors," *Tech. Rep. MIT-ANP-TR-100*, pp. 1–317, 2004.

[15] D. Alfani, M. Astolfi, M. Binotti, S. Campanari, F. Casella, and P. Silva, "Multi objective optimization of flexible supercritical CO2 coal-fired power plant," *ASME Turbo Expo 2019 Turbomach. Tech. Conf. exibition*, pp. 1–11, 2019.

[16] "Thermoflow." 2016.

[17] F. W. Dittus and L. M. K. Boelter, "Heat transfer in automobile radiators of the tubular type," *Int. Commun. Heat Mass Transf.*, vol. 12, no. 1, pp. 3–22, Jan. 1985.

[18] A. S. L. Frank P. Incropera, David P. DeWitt, Theodore L. Bergman, "Fundamentals of Heat and Mass Transfer.pdf," *USA: John Wiley & Sons. ISBN*, vol. 13. Wiley, p. 997, 2002.

[19] D. Alfani, M. Astolfi, M. Binotti, E. Macchi, and P. Silva, "Part-Load Operation Of Coal Fired sCO2 Power Plants," in *3rd European supercritical CO2 Conference September 19-20, 2019, Paris, France*, 2019, pp. 1–9.

[20] E. Gimon *et al.*, "The coal cost crossover: economic viability of existing coal compared to new local wind and solar resources," 2017.

[21] D. Wamsted and S. Feaster, "Coal-Fired Power Generation in Freefall Across Southeast U.S. One-Two Combination of Gas and Solar Is Pushing Historically Dominant Industry Aside," 2019.

[22] B. Caldecott *et al.*, "The fate of European coal-fired power stations planned in the mid-2000s: Insights for policymakers, companies, and investors considering new coal," 2017.

[23] C. Tran, "Capacity factors: Understanding the misunderstood," *Australian Energy Council*.

[24] "TERNA Transparency Report: Actual Generation 2017." [Online]. Available: https://www.terna.it/it/sistema-elettrico/transparency-report/actual-generation.

[25] D. Alfani, M. Astolfi, M. Binotti, and P. Silva, "D5.3 - First Annual Performance in Steady State and Operation Range,". December 2019, 2020.